

## Density estimations using density-velocity relations and seismic inversion

Maria F. Quijada and Robert R. Stewart

### ABSTRACT

Density can be an important parameter to differentiate lithologies and estimate other petrophysical properties, such as porosity or fluid content. Density in the area has a complex behavior, not related directly to lithology; with the best lithological indicator being the  $V_p/V_s$  ratio. Also, density changes within the interval of interest can generate significant changes in the amplitudes and their variations with offset. Density, gamma-ray, P- and S-wave sonic data from a well in Manitou Lake, Saskatchewan were used to evaluate different density-velocity relations and their parameters. Default values for  $a$  and  $m$  in Gardner's equation are 0.31 and 0.25, respectively. Using a local fit for sands and shales, differentiated using the GR log, results in values of  $a$  and  $m$  of 0.51 and 0.19 for shales, and 0.22 and 0.28 for sands. Using Lindseth's approach the biggest change is on parameter  $d$ , which changes from 1054 to 855 for sands, and to 459 for shales. The RMS value of the residuals using Gardner's equation is improved from 0.1147 to 0.0879 g/cm<sup>3</sup> just by estimating parameters from a local fit, while the difference is even greater when using Lindseth's equation, changing from 0.4550 to 0.0879 g/cm<sup>3</sup>. Densities estimated from impedance show similar RMS errors, but using the parameters from the single fit results in an averaged log with no variations associated to the geology.

### INTRODUCTION

Estimating density values from seismic data has remained an elusive task, as the inverse problem is ill-posed, with a small change in the data resulting in a large change in the solution. In general, two parameters (i.e., P- and S-impedance, or P- and S-wave velocity) can be reasonably estimated from PP and PS seismic inversion (Downton, 2005; Mahmoudian, 2006). However, inversion for a third parameter, such as rock density, is unstable even in the case of moderately noisy data, requiring the inclusion of a constraint on the parameters, usually by including a density-velocity relation, to stabilize the inversion (Wang, 1999).

The bulk density of a rock is a function of mineral composition, porosity, water saturation and hydrocarbon fluid type. It can provide essential information for delineating a reservoir or planning the position of a new producing or injecting well. Cross-plots between rock properties and lithology and pore fluid indicate that density provides the best differentiation between hydrocarbon reservoirs and other rock/fluid types (Van Koughnet et al., 2003), making accurate density estimates significant for reservoir characterization.

Well logs are used to evaluate different density-velocity equations, including Gardner's and Lindseth's relationship, for estimating density, both from P- and S-wave velocities. Band-limited inversion is performed on synthetic traces to estimate density using these relations. The logs and seismic data used are from Manitou Lake, Saskatchewan, near the Lloydminster area (Figure 1).

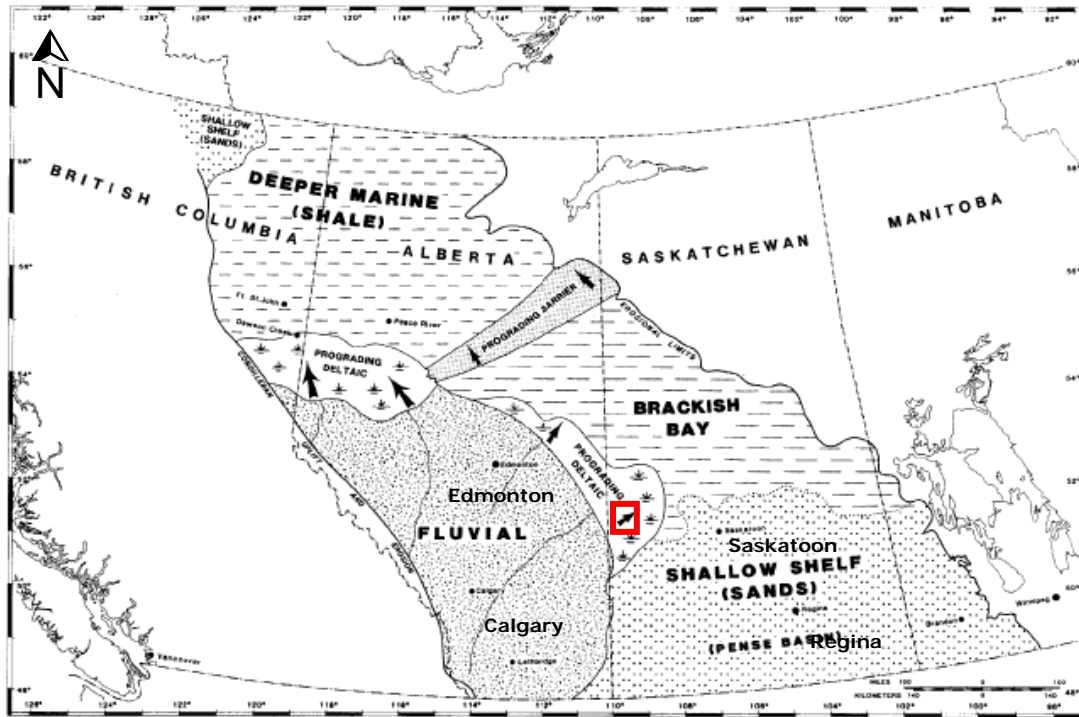


FIG. 1. Paleogeographic reconstruction of the Upper Mannville deposition. Red square shows location of the area of study (Modified from Leckie and Smith, 1992).

## GEOLOGIC SETTING

Deposition in the Western Canada Sedimentary Basin (WCSB) can be divided into two successions, based on two different tectonic settings affecting sedimentation. The Paleozoic to Jurassic platformal succession, dominated by carbonate rocks, was deposited on the stable craton adjacent to the ancient margin of North America. The overlying mid-Jurassic to Paleocene foreland basin succession, dominated by clastic rocks, formed during active margin orogenic evolution of the Canadian Cordillera, with the emplacement of imbricate thrust slices progressively from east to west (Mossop and Shetsen, 1994).

Figure 2 shows the stratigraphic column for west-central Saskatchewan, with the red arrows showing the exploration targets in the area, corresponding to the Colony sand member of the Pense Formation, and the Sparky member of the Cantuar Formation, both part of the Cretaceous Mannville Group. The top of the Mannville marks a clear separation between the predominant sands in the group and the overlying marine shales of the Colorado and Belly River Groups.

The Colony sand member consists of shales, siltstones, coals and sandstones. Deposition of this member occurred in an extensive complex of anastomosing channels sandstones, encased within siltstones, shales, coals and thin sheet sandstones (Putnam and Oliver, 1980). The Sparky member is informally grouped into the middle Mannville, which is dominated by sheet sandstone development, with narrow, channel sandstones and shales also present (Putnam, 1982). These units have been interpreted as a delta-front



Table 1. Statistics of density distributions of several rock types in Alberta using compensated density logs (Modified from Maxant, 1980).

Rock type	Number of samples	Mean (g/cm <sup>3</sup> )	Median (g/cm <sup>3</sup> )	Mode (g/cm <sup>3</sup> )	Standard deviation (g/cm <sup>3</sup> )
Sandstone	667	2.42	2.45	2.5	0.18
Siltstone	73	2.46	2.55	2.6	0.19
Shale	943	2.43	2.46	2.52	0.19
Limestone	337	2.63	2.67	2.69	0.15
Dolomite	257	2.64	2.67	2.69	0.16

## GEOPHYSICAL DATA

The data used in this project includes a suite of logs from three different wells in the Manitou Lake area, and seismic data from a 3C-3D survey in the area. The seismic data were acquired for Calroc Energy Inc. by Kinetex Inc. in February 2005, covering an area of approximately 10 km<sup>2</sup>, with twenty one south-north receiver lines and eighteen west-east source lines (Figure 3), with 200 m line spacing and 50 m station spacing (Lu et al., 2006). The exploration targets of this survey include the Colony and Sparky members of the Mannville Group.

Three wells were available for this study (A11-17-44-27, C07-16-44-27 and C10-17-44-27) with a suite of logs, including gamma-ray (GR), spontaneous potential (SP), density (RHOZ), neutron and density porosity, caliper, and resistivity, among others. Wells A11-17 and C07-16 both have P-wave sonic, while an S-wave sonic is available for well A11-17. Well A11-17 is producing from the Colony member, while the other two wells produce from the Sparky B interval. In the following sections, results will be shown for well A11-17.

Figure 4 shows the logs from well A11-17. Note the sharp contrast in the GR, SP and Vs at the top of the Colony sands, around 550 m. As expected from the geology, the GR shows high values indicative of shales above the Colony tops and lower GR values in the Mannville group. P-wave velocity shows little change at the top of the Mannville, suggesting it is not a good lithological indicator. High resistivities in the Colony and Sparky members indicate hydrocarbons, while the cross-over between the density and neutron porosity logs in the Colony sands could indicate gas. Several coal beds can be interpreted in the area, based on the very low density values, between 1.6 and 1.7 g/cm<sup>3</sup>.

Note that at the top of the Mannville the density and the velocity logs appear to be anticorrelated, with a significant decrease in the density and an increase in the velocity values. This is especially obvious in the case of the S-wave. Also, the general trend of the velocities is to increase with depth, while the densities decrease with depth. High resistivities, usually indicative of hydrocarbons, occur in the Colony and Sparky members.

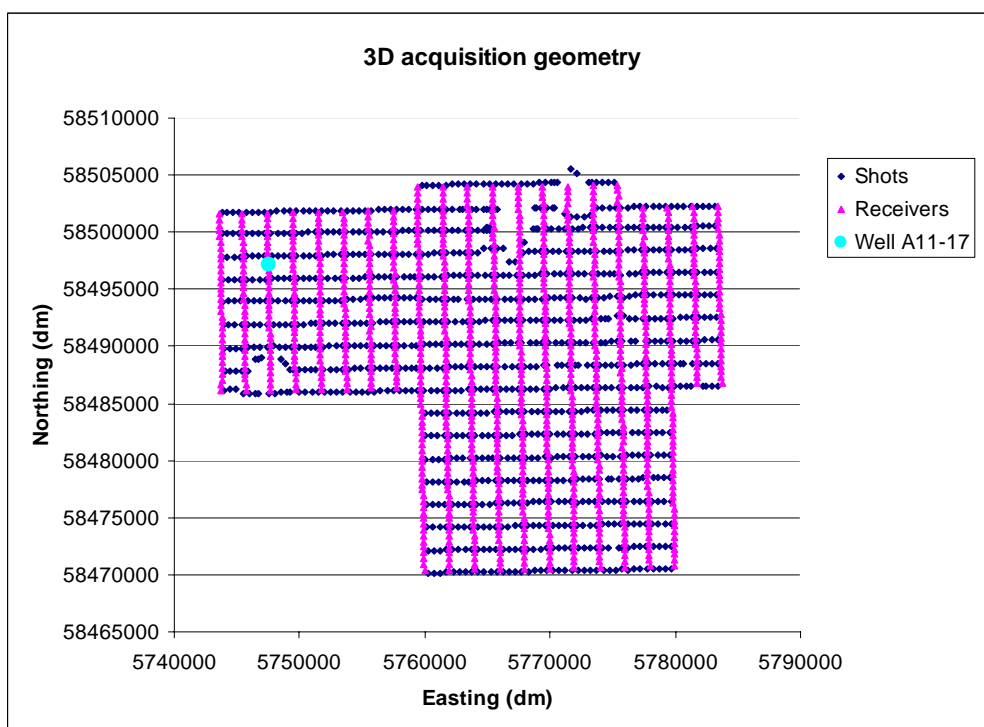


FIG. 3. Acquisition geometry for the Manitou Lake Survey. Shots are in blue, Receivers in magenta, and well A11-17 is the cyan circle.

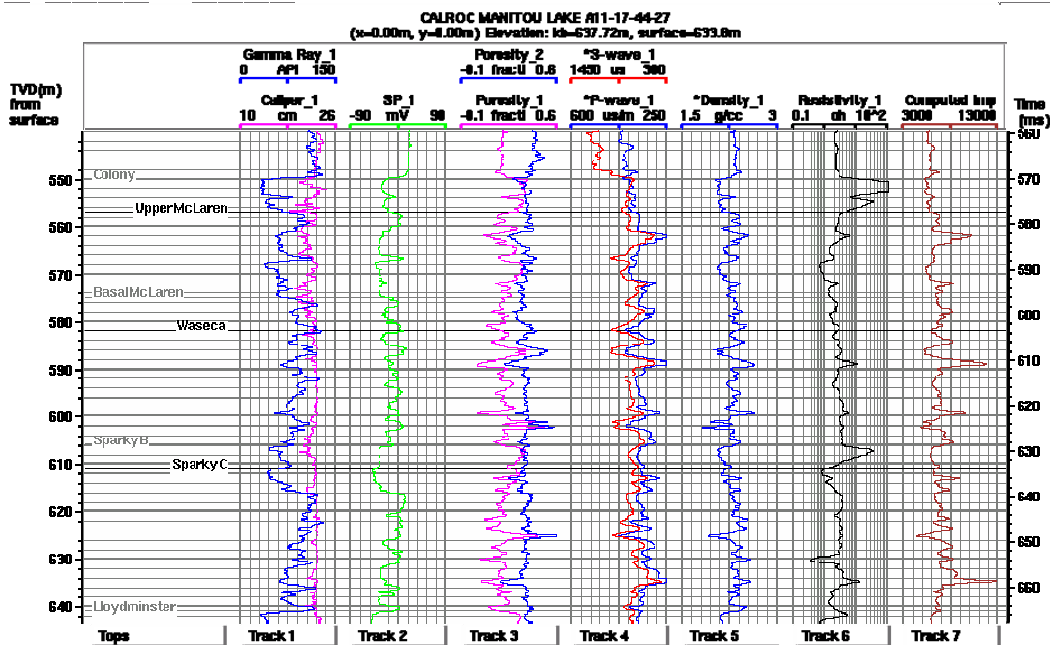


FIG. 4. Logs from well A11-17.

## DENSITY ESTIMATES

Density can be estimated from seismic data by seismic inversion (i.e. AVO or waveform inversion) or by geostatistical methods, where linear (i.e. multi-linear regression) or non-linear (i.e. neural networks) relationships can be established between the rock properties, calculated at the well location, and the seismic data or a specific seismic attributes. In general, the lithological and fluid properties of a medium cannot be inferred from P-wave data alone, requiring information from the S-wave response (Barnola and White, 2001).

Petrophysical analysis shows that bulk density is an important acoustic indicator of the presence of shale. In the case of oil sands or heavy oil developments, accurate estimates of density are necessary to determine the location of shales in the reservoirs, which may interfere with the steaming or recovery process (Gray et al., 2006). Coal density varies with ash and water content, and rank (Ryan, 2006). In general, higher ash content implies a higher specific gravity and lower gas content, making density a key factor in determining the quality of the coal.

### Density-velocity relations

Gardner et al. (1974) found an empirical relationship between density and velocity from a series of controlled field and laboratory measurements of brine-saturated rocks, excluding evaporites, from various locations and depths, given by:

$$\rho = aV^m \quad (1)$$

where  $\rho$  is density and  $V$  is P-wave velocity. Default values for  $a$  and  $m$  are 0.31 and 0.25, respectively, for density in  $\text{g/cm}^3$  and P-wave velocity in m/s. Gardner's relation is a good approximation for shales, sandstones and carbonates, while coals and evaporites depart significantly from the expected behavior.

Taking logarithm on both sides of equation (1) gives a linear relationship between  $\log(\rho)$  and  $\log(V)$ , making it possible to use a linear regression to find the coefficients  $a$  and  $m$  that best fit the data in a least squares sense, according to the following equation:

$$\log(\rho) = \log(a) + m \log(V) \quad (2)$$

Figure 5a shows the plot of  $\log(\rho)$  vs  $\log(V)$  for well A11-17, showing the least-squares fit to equation 2. Velocities are in m/s and density is in  $\text{g/cm}^3$ . Note that the points appear to be differentiated in two clusters, with differentiated GR values. A single fit for all points results in a value of  $a$  and  $m$  of 0.927 and 0.11, respectively; which are significantly different from Gardner's default parameters. Also, there is considerable dispersion of the points from the straight line. The points with very low densities correspond to several coal seams within the Mannville interval.

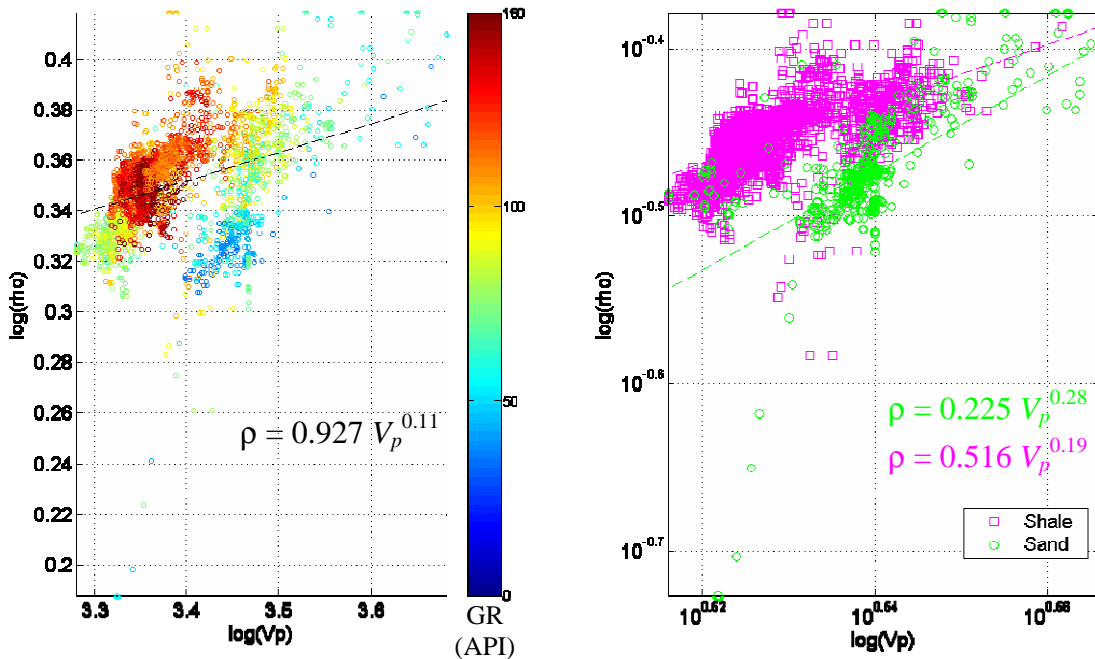


FIG. 5. Crossplot of  $\log(\rho)$  vs  $\log(V_p)$  for well A11-17.

Castagna et al. (1993) suggest using values of  $a$  and  $m$  specific to each rock type. The stratigraphic column shows that shale is the dominant lithology above the top of the Mannville, except for a few interbedded sandstones, while sediments within the Mannville Group are predominantly sands. The Gamma Ray log supports this lithological separation, showing a sharp decrease correlated to the Mannville top. Based on this, the GR was used as a lithology discriminator, to estimate values of  $a$  and  $m$  for specific rock types. Samples with GR values below 70 API were considered sands and higher values shale. Using this constraint, two sets of values were calculated for each rock type. Using this constrain, the graph was replotted with samples in green having GR lower than 70 while samples in magenta have GR higher than 70, note that the two clusters are now clearly differentiated, with very little overlap between the samples. The fit is significantly improved by using this separation, with less dispersion of points with respect to the fitted line and coefficients closer to those defined by Gardner.

Figure 6 shows the estimated density log using Gardner's relation with the different coefficients. Using Gardner's default parameters gives a very poor fit in the shale section of the log, but improves significantly within the Mannville interval; however, the behavior of the log at the top of the Mannville is opposite to the original log, showing an increase in density, instead of a sharp decrease. The parameters estimated from a single fit result in a very averaged density log, showing only very small fluctuations. The best density log is obtained using specific parameters for the two predominant rock types, especially within the Mannville interval, honoring the sharp decrease in density at the top and other fluctuations.

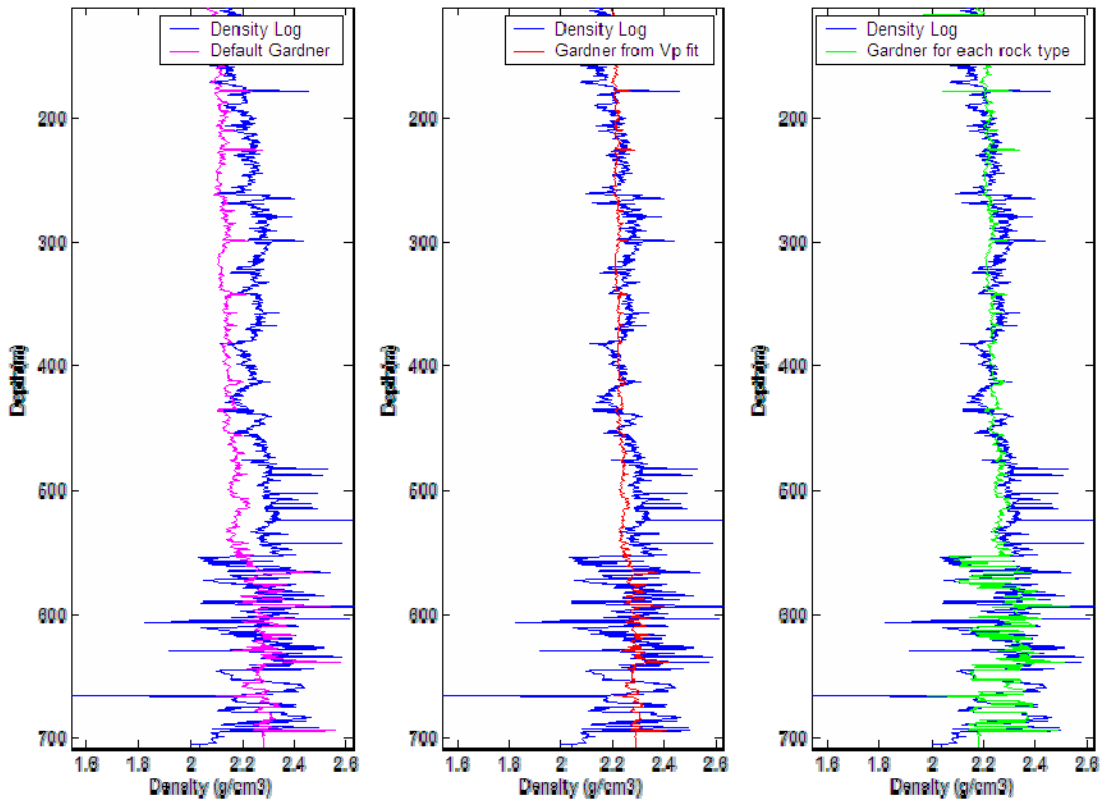


FIG. 6. Density estimates for well A11-17 using Gardner's equation (a) using default values of  $a$  and  $m$ ; (b) using single fit for  $V_p$ , and (c) using  $a$  and  $m$  specific for sand and shale.

Figure 7 shows a series of crossplots from the logs in well A11-17, the blue ellipses represent low GR regions and yellow ellipses high GR regions. Note that density is not a good lithological indicator, as density values overlap for sands and shales, in a range between 1.7 and 2.4 (Figure 7a and 7c).  $V_p$  also shows overlap between sands and shales, with shales having a generally lower velocity than the sands. On the other hand, S-wave velocity shows very little overlap and appears to be the best lithological indicator, along with the  $V_p/V_s$  ratio (Figure 7b and 7c), where sands have a ratio between 1.7 and 2.4, and shales between 2.4 and 4.

Given the linear behavior observed between impedance and velocity (Figure 7d), Lindseth's empirical relation was evaluated. Lindseth (1979) derived a linear empirical relation between velocity and impedance, given for velocity in ft/s and  $\rho$  in  $\text{gr}/\text{cm}^3$  by:

$$V = 0.308\rho V + 3460 \quad (5)$$

When considering velocity in m/s, the coefficients become 0.308 and 1054.

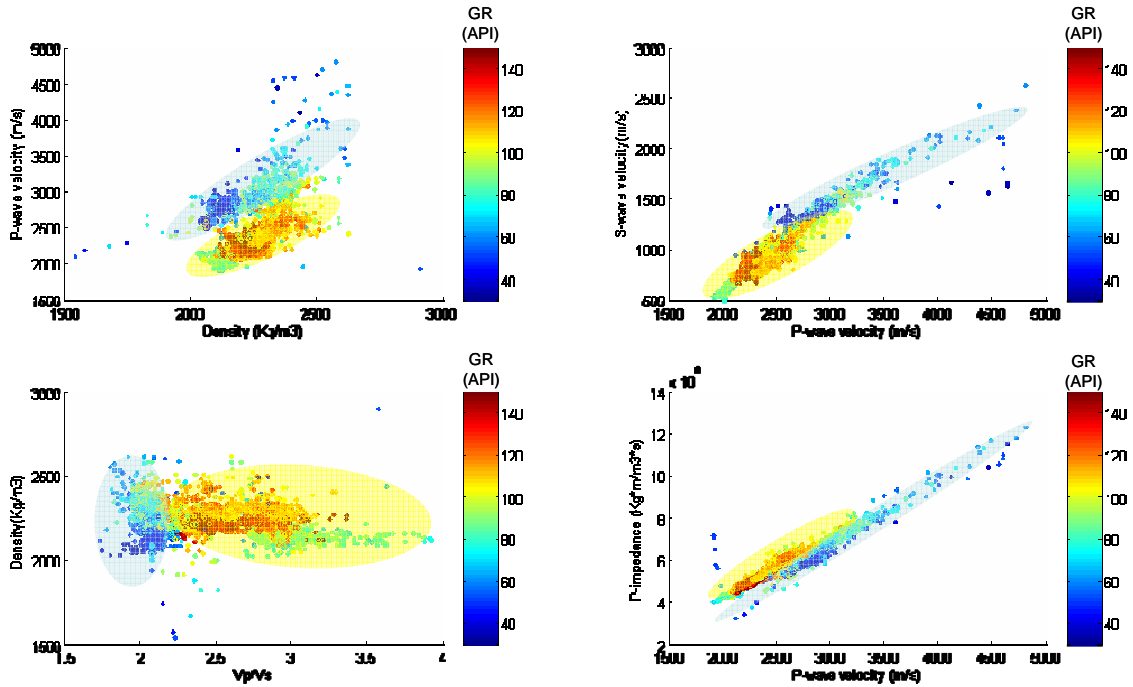


FIG. 7. (a) P-wave velocity vs. density; (b) S-wave velocity vs. P-wave velocity; (c) Density vs. Vp/Vs, and (d) P-Impedance vs. P-wave velocity for well A11-17. Yellow ellipses indicate higher GR values, while blue ellipses represent low GR values.

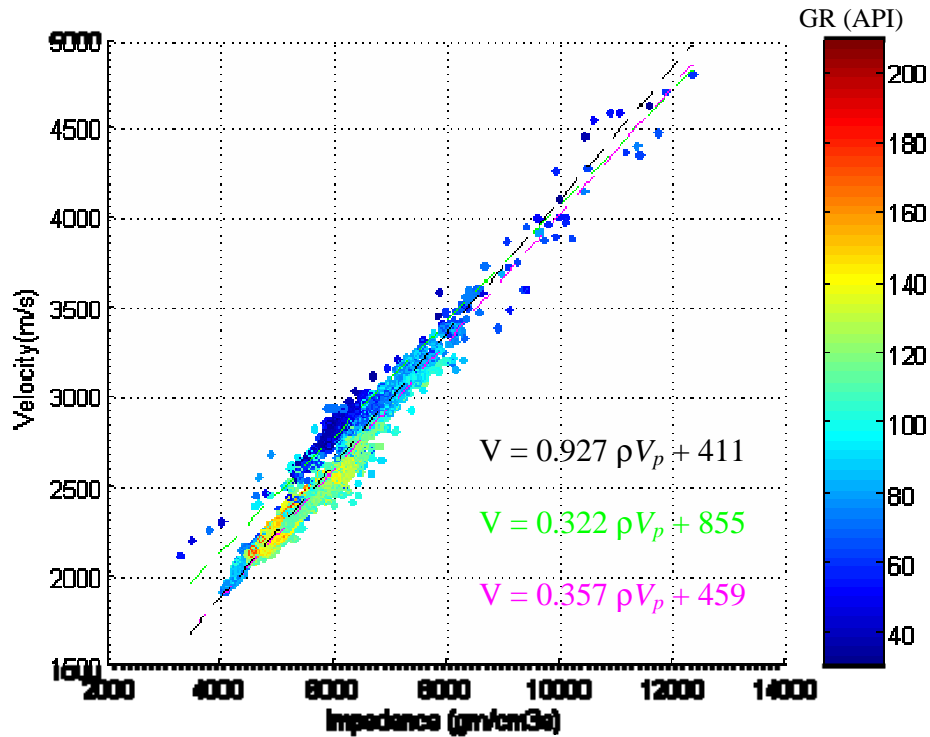


FIG. 8. Velocity vs. P-impedance cross-plot showing linear fit for all points (black), for sands (green) and for shales (magenta).

Using a least-square linear fit for the equation  $V = c\rho V + d$  (5), the coefficients  $c$  and  $d$  that best fit the data are calculated for both wells. Solving for density in equation (5) results in:

$$\rho = \frac{V - d}{cV} \quad (6)$$

Figure 8 shows the results of different fits for equation 5, which were subsequently used to calculate different density logs (Figure 9). Lindseth's default parameters (magenta line) give a very poor approximation of the density log, especially in the shale interval, where the residual is as big as  $0.6 \text{ g/cm}^3$ . Using the single fit (red line) improves the density estimates; however, it shows the same issues as Gardner's single fit, resulting in a very averaged log and showing an increase in density at the top of the Mannville. Finally, the best density log is obtained by using different parameters for sands and shales (green line).

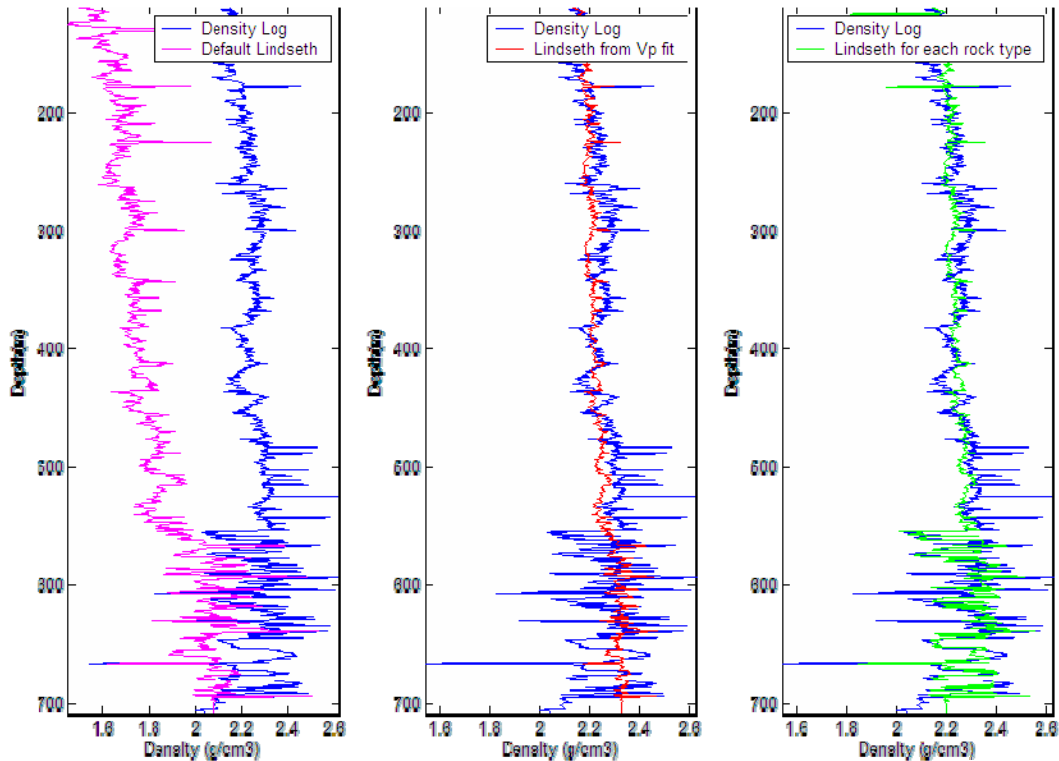


FIG. 9. Density estimates using Lindseth's linear relation between velocity and impedance for well A11-17 (a) using default parameters; (b) single fit between  $I_p$  and  $V_p$ , and (c) using different parameter for sand and shale.

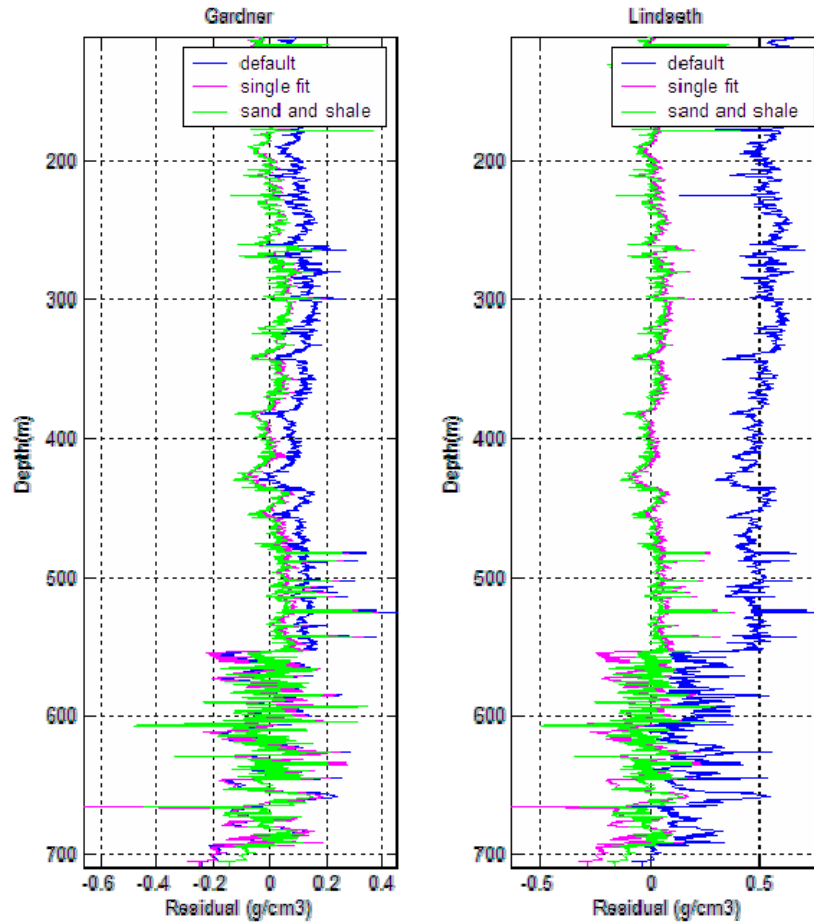


FIG. 10. Residual density for Gardner's and Lindseth's relations.

Table 2 summarizes the results from using the different density-velocity relations to estimate density. Note the significant improvement by fitting the data locally instead of using the default parameters, especially when using Lindseth's equation. The best results were obtained when using specific parameters for sand and shale, with very little difference between selecting Gardner's or Lindseth's approach. The best fit is obtained for the shale section in both cases, probably due to the very small fluctuations in density within this interval. Lindseth's equation does a better work at modeling the very low densities associated to the coal seams within the Mannville, as in Gardner's approach the points with very low densities are not within the fitted trend to the data.

The forward modeling done shows that when using density-velocity relations it is necessary to evaluate which equation best fits the data and parameters should be estimated locally, as most of these equations were derived empirically and the coefficients are significantly affected by local geology. Density and velocity can give information about different elastic parameters of the rocks, and using these relations might result in a loss of information. For example, density can be easily related to the pore fluid density and the porosity, while the velocity is not simply related to the porosity (Barnola and White, 2001), mostly due to the presence of microcracks, which strongly affect the P- and S-wave velocities (Mavko et al., 1998).

Table 2. Gardner's and Lindseth's coefficients obtained using different fits to the data, showing RMS value of the density residuals.

Fit	A	M	RMS error (g/cm <sup>3</sup> )
Gardner's coefficients	0.310	0.25	0.1147
Gardner's single fit	0.9277	0.1131	0.0848
Gardner's fit for shale	0.5162	0.1896	0.0583
Gardner's fit for sand	0.2249	0.2847	0.0678
Fit	C	D	RMS error (g/cm <sup>3</sup> )
Lindseth's coefficients	0.308	1054.06.	0.4550
Lindseth's single fit	0.3702	411.09	0.0879
Lindseth for shale	0.3572	459.25	0.0579
Lindseth for sand	0.3224	855.37	0.0708

### Seismic inversion

Synthetic data was generated from the well logs available, in order to evaluate the effect of including different density-velocity relations in density estimates from inverted impedances. The synthetic trace was generated using the function *theosimple* from Matlab, which calculates a 1-D synthetic seismogram using a convolutional model. A Ricker wavelet with a dominant frequency of 80 Hz was used, as this is the dominant frequency of the P-P data from the Manitou Lake survey. The sampling interval was set to 0.001 s and no multiples or transmission losses are included in the model.

The seismic inversion was performed using the BLIMP algorithm in Matlab (Ferguson and Margrave, 1996), which calculates a band limited impedance from the zero offset reflectivity, using a recursive approach. The normal incidence reflection coefficients ( $R_i$ ) are defined in terms of the impedance ( $I_i$ ) as:

$$R_i = \frac{I_{i+1} - I_i}{I_{i+1} + I_i} \quad (7)$$

Solving for  $I_{i+1}$ , taking the natural logarithm, making an approximation for small  $R$  and modelling the seismic trace as a scaled reflectivity ( $S_k = 2R_k / \gamma$ ), equation (7) converts to:

$$I_{i+1} = I_1 \exp\left(\gamma \sum_{k=1}^i S_k\right) \quad (8)$$

The inversion is performed using an approach similar to that of Waters (1978). An initial impedance estimate is calculated from the well logs, and the seismic trace is integrated and exponentiated, according to equation 8. The Fourier spectrum of the

integrated trace is scaled to that of the estimated impedance and a low-pass filtered impedance is added to the trace. The result is transformed to the time domain, and a new impedance estimate is obtained. In this case, the low- and high-cut frequencies were set to 10 and 80 Hz, respectively.

To calculate density from impedance it is necessary to know the velocity. In this case, the density-velocity relations evaluated previously will be used to estimate the density from impedance. Assuming Gardner's relation is valid, the expression for velocity in terms of density is:

$$V = \left( \frac{\rho}{a} \right)^{\frac{1}{m}} \quad (9)$$

and substituting this equation into equation  $I = \rho V$ , and solving for density results in:

$$\rho = (aI^m)^{\frac{1}{m+1}} \quad (10)$$

Using Lindseth's equation, velocity is expressed in terms of density as:

$$V = \frac{d}{1 - c\rho} \quad (11)$$

and solving for density as in the previous case:

$$\rho = \frac{I}{d + cI} \quad (12)$$

Equations 10 and 12 were used to estimate density from the inverted impedances calculated using BLIMP. In general, the estimated impedance is smoother than the real impedance, showing less detail and fluctuations, but maintaining the same trend. As a consequence, the density estimates are also be smoother than the actual density. As seen with the modeling, when using a single fit to Gardner or Lindseth, the estimated density is an average of the original density log, showing very little detail, and when using Gardner's default parameter a good fit is obtained only in the Mannville interval (Figure 11). Note that the inverted impedance

Using specific coefficients for sands and shales results in a more accurate density estimates, although the band limited nature of the inversion results in a smoother density curve (Figure 12). Note that there is very little difference between selecting Gardner's or Lindseth's approximation. Once again, the low densities associated to the coals cannot be inverted properly with either approach.

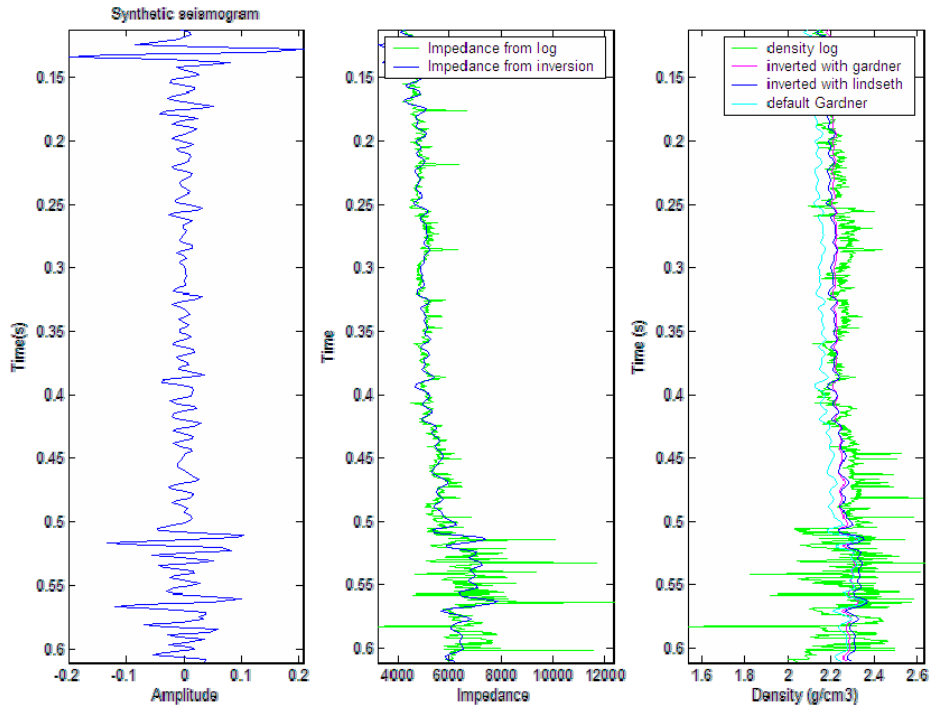


FIG. 11. Density estimated from the inversion of the impedance log using Gardner's and Lindseth's relations with the coefficients from the single fit.

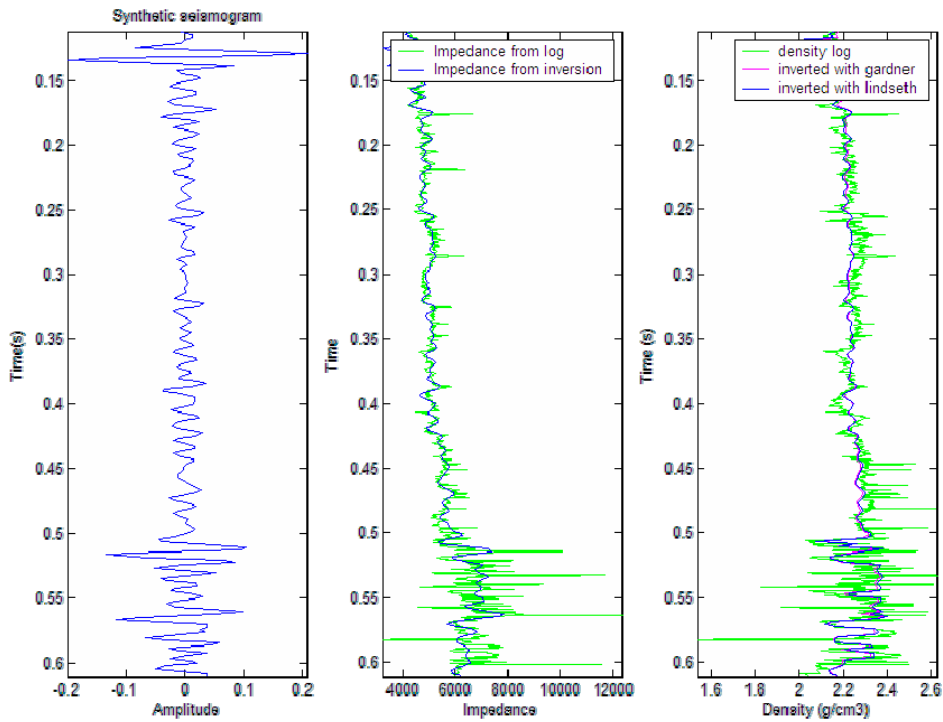


FIG. 12. Density estimated from the inversion of the impedance log using Gardner's and Lindseth's relations with the coefficients for sand and shale.

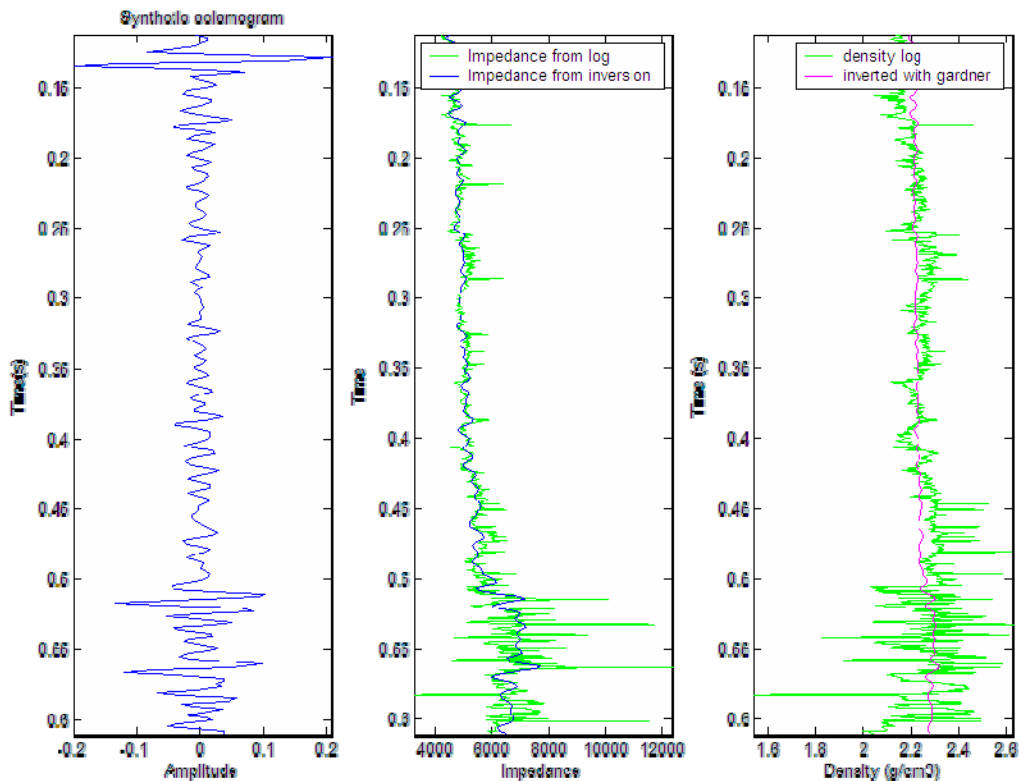


FIG. 13. Impedance inversion using initial impedance calculated with Gardner's density.

The first inversions were performed using an initial impedance calculated from the true well logs. To evaluate the effect of using density-velocity relations to generate initial models, when not all logs are available, another inversion was performed using Gardner's relation when estimating the initial impedance for BLIMP. Figure 13 shows the result from this inversion, and it is possible to see that the inverted impedance is very similar to the one estimated previously, even in the case when using the single fit for estimating the coefficients. This shows that density-velocity relations, even when using parameters, are good approximations to generate initial models for the inversion. However, when estimating density from the impedance it is necessary to use parameters calculated for each rock type, to obtain accurate density values.

Table 3 shows the RMS error of the estimated densities from the inverted impedances using the two density-velocity relations. Note the magnitude of the errors is similar to those obtained from the forward modeling, being slightly lower than the previous values. This improvement in the fit is probably due to the use of the real density log in the initial impedance estimate supplied to the program. Even though the errors for the single fit and those from the sand and shale coefficients are very similar, visual inspection of the results clearly shows that a significantly better fit is obtained using different coefficients for each rock type, with the single fit showing a very average behavior and very little fluctuations reflection the geology of the area.

Table 3. RMS errors of density estimations from impedance inversion, using different density-velocity relations.

<b>Inversion</b>	<b>RMS error (g/cm<sup>3</sup>)</b>
Inversion with Gardner's coefficients	0.1032
Inversion with Gardner's single fit	0.0838
Inversion with Gardner's fit for shale and sand	0.0720
Inversion using initial impedance from model	0.0863
<b>Inversion</b>	<b>RMS error (g/cm<sup>3</sup>)</b>
Inversion with Lindseth's single fit	0.0836
Inversion with Lindseth's fit for shale and sand	0.0720

## CONCLUSIONS

Inspection of the well logs available shows that the S-wave velocity and P-wave velocity are linearly correlated, except at the top of the Mannville, where  $V_s$  shows a sharp increase not seen in the P-wave velocity. In this area,  $V_s$  and  $V_p/V_s$  appear to be the best lithological indicators, showing very little overlap in the values between sands and shales. Density has a more complex behavior, as it appears to be anticorrelated with the velocity in the interval of interest, and it is not a good lithological indicator, with considerable overlap in values for sands and shales. However, it could be indicating variations in other petrophysical properties, such as porosity or fluid saturation. Further modeling is necessary to evaluate the effects of these properties on density.

In order to use density-velocity relations it is recommended to evaluate the relations between the different logs and properties and obtain parameters from a local fit to the data. The parameters obtained from a single fit can be adequate to generate initial models for the inversion process; however, if density is to be estimated from impedance using these relations it is necessary to use specific parameters for each rock type to obtain more accurate results.

Using density-velocity relations to constraint seismic inversion can introduce biases in the results. By performing a full waveform inversion, considering three independent parameters, more information about the subsurface can be retrieved from the seismic data, while introducing fewer biases in the inversion process.

## Future Work

The following step is to perform a full waveform seismic inversion of the data from Manitou Lake, which will allow the calculation of elastic rock properties, using both amplitude and traveltime information, by minimizing the differences between observed and calculated seismic data. Waveform inversion provides a convenient framework to deal with the fact that PP and PS data have different wavelets, while also avoiding NMO

stretch and offset dependent tuning problems associated with the inclusion of far-offset data in AVO inversions (Downton, 2005). Three major steps are involved in the inversion: forward modeling, optimization procedure and uncertainty analysis.

Figure 14 shows the raw shot gathers from the selected receiver line, showing the vertical and the horizontal components. Note the presence of high amplitude events in the vertical component between 600 and 800 ms and deeper in the section between 1200 and 1400 ms. The radial component shows some coherent events in the deeper part of the section, below 1100 ms.

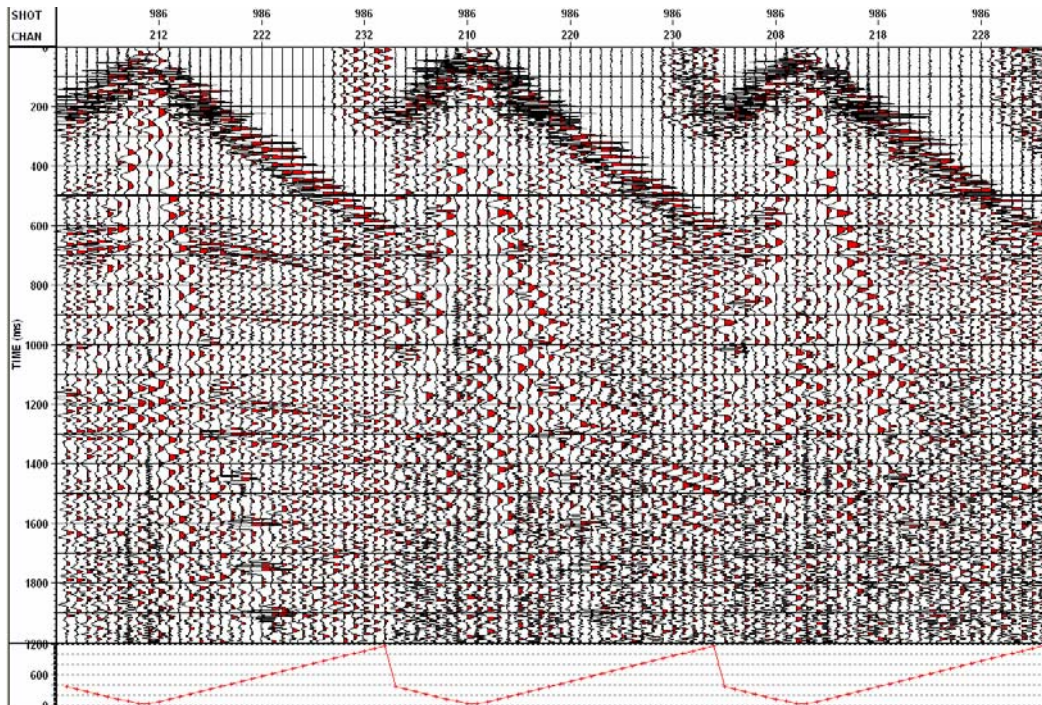


FIG. 14. Raw shot gathers from the Manitou Lake survey (a) Vertical component; (b) and (c) radial components.

Waveform inversion can be implemented both in the time or frequency domain. The choice of a domain for inversion allows one to apply specific methodologies to precondition the data residuals or the gradient, in ways that may improve the convergence or the linearity of the inverse problem (Sirgue and Pratt, 2003). Even though the problem is highly non-linear, different approaches using both linear and non-linear approximations have been applied. Non-linear methods have very high computational requirements and lower resolution due to the sparse parametrization of the subsurface, but they require little a priori information. On the other hand, linear methods produce higher resolution results but require a good initial model. Local and global optimization methods are used in seismic waveform inversion. Traditionally, local methods (conjugate-gradient and downhill simplex methods, among others) have been preferred over the global approach (genetic algorithms, simulated annealing) due to computational cost, although they require an initial model very similar to the optimal answer. The main problems arise from the presence of several local minima in the objective function, which

prevent iterative optimization techniques to work effectively, which can require the construction of constrained objective functions.

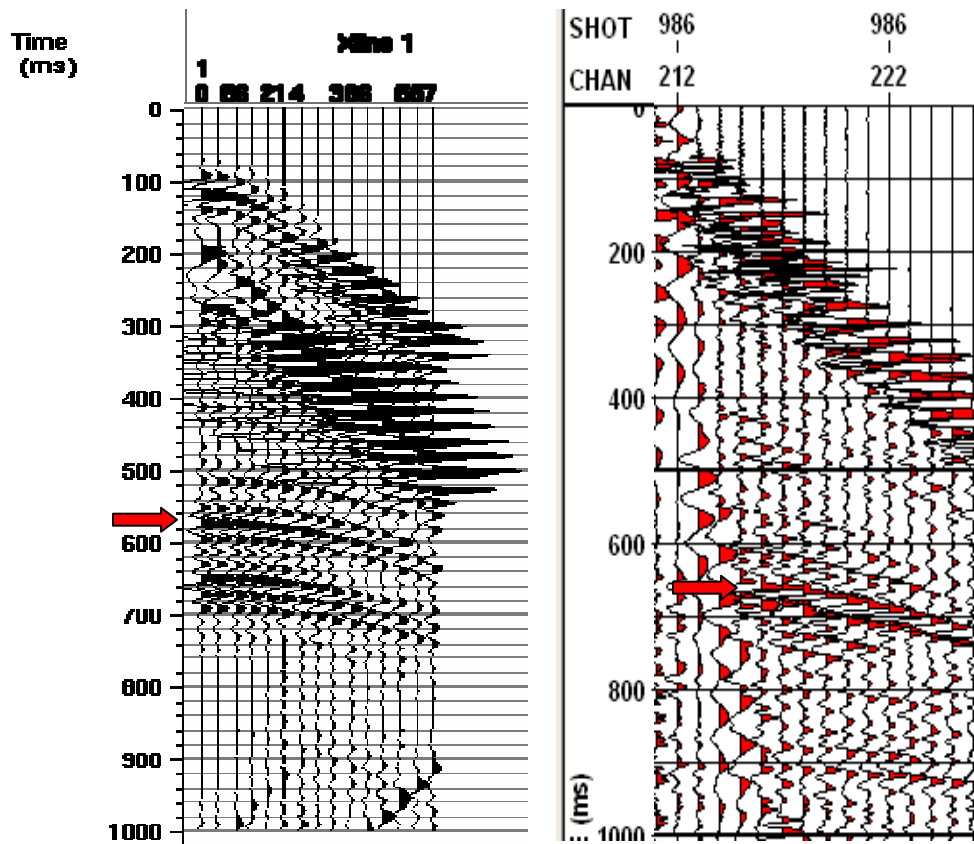


FIG. 15. Comparison of modeled shot gather using the reflectivity method (vertical component) with the raw shot gather.

Figure 15 shows a comparison between the vertical component of a modeled shot gather using the reflectivity method and the vertical component from a raw shot gather close to the well. Note there seems to be a correlation between events, but they are located at different times (red arrows in figure 15). In this case, a synthetic has not been tied to the seismic and there is no check-shot information to provide information about the near surface velocity. An adequate correlation of events must be made before any residuals can be calculated.

Figure 16 shows a set of modeled shot gathers from well a11-17 showing density variations within the Colony sand from 2 to 3 g/cm<sup>3</sup>. Note there is a significant change in the amplitudes and their variations with offset as density changes.

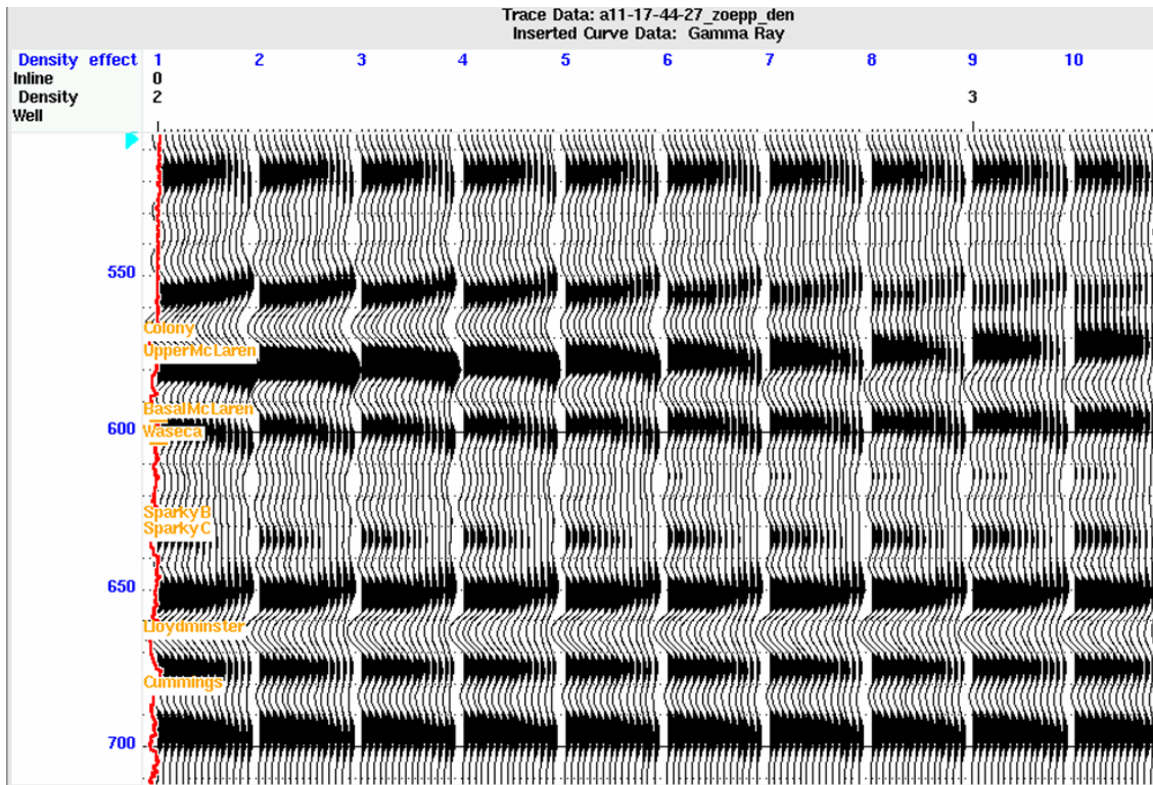


FIG. 16. Synthetic shot gathers showing density variations from 2 to 3 g/cm<sup>3</sup> within the Colony member.

### ACKNOWLEDGEMENTS

We would like to thank Calroc Energy Inc. for providing this dataset to CREWES and Veritas Hampson-Russell (VHR) for the use of donated software (Geoview). We also would like to thank CREWES sponsors for their financial support.

### REFERENCES

- Barnola, A.S., and R.E. White, 2001, Gardner's relation and AVO inversion: *First Break*, **19**, 607-611.
- Castagna, J.P., M.L. Batzle, and T.K. Kan, 1993, Rock physics - The link between rock properties and AVO response in Castagna, J.P., and M. Backus, *Offset dependent reflectivity, Theory and Practice of AVO analysis*: SEG, 135-171.
- Downton, J., 2005, *Seismic parameter estimation from AVO inversion*: Ph.D Thesis, University of Calgary.
- Ferguson, R. J., and G.F. Margrave, 1996, A simple algorithm for band-limited impedance inversion: CREWES Research Report, **8**.
- Gardner, G. H. F., L. W. Gardner, and A. R. Gregory, 1974, Formation velocity and density—the diagnostic basics for stratigraphic traps: *Geophysics*, **39**, 770–780.
- Gray, F. D., P. Anderson, and J. Gunderson, 2006, Prediction of Shale Plugs between Wells in Heavy Oil Sands using Seismic Attributes: *Natural Resource Research*, **15**, no. 2, 102-109.
- Kelly, M., and C. Skidmore, 2001, Non-linear AVO equations and their use in 3- parameter inversions: 71st Annual International Meeting, SEG, Expanded Abstracts, 255-256.
- Lindseth, R.O., 1979, Synthetic sonic logs – A process for stratigraphic interpretation: *Geophysics*, **44**, 3-26.
- Lu, H.X., K. Hall, R.R. Stewart, D. Feuchtwanger, and B. Szatkowski, 2006, Searching for sand reservoirs: Processing 3C-3D seismic data from Manitou Lake, Saskatchewan: CREWES Research Report, **18**.

- Mahmoudian, F., 2006, Linear AVO inversion of multi-component surface seismic and VSP data: M. Sc. Thesis, University of Calgary.
- Maxant, J., 1980, Variation of density with rock type, depth, and formation in the Western Canada basin from density logs: *Geophysics*, **45**, 1061-1076.
- Mossop, G.D. and I. Shetsen (comp.), 1994, Geological atlas of the Western Canada Sedimentary Basin; Canadian Society of Petroleum Geologists and Alberta Research Council, Calgary, Alberta, URL [http://www.ags.gov.ab.ca/publications/ATLAS\\_WWW /ATLAS.shtml](http://www.ags.gov.ab.ca/publications/ATLAS_WWW /ATLAS.shtml), [April 15th, 2006].
- Putnam, P.E. and T. A. Oliver, 1980, Stratigraphic traps in channel sandstones in the Upper Mannville (Albian) and east-central Alberta. *Bulletin of Canadian Petroleum Geology*, **28**, 489-508.
- Royle, A. J., 2002, Exploitation of an oil field using AVO and post-stack rock property analysis methods: 72nd Annual International Meeting, SEG, Expanded Abstracts, **21**, 289-292.
- Ryan, B., 2006, Coal Basics for CBM in Coal Bed Methane: An integrated Approach to Reservoir Characterization and Production. 2006 CSPG/CSEG/CWLS Joint Convention Short Course.
- Sirgue, L., and R. G. Pratt, 2003, Efficient waveform inversion and imaging: A strategy for selecting temporal frequencies: *Geophysics*, **69**, 231-248.
- Van Koughnet, R. W., C. M. Skidmore, M. C. Kelly, and R. Lindsay, 2003, Prospecting with the density cube: *The Leading Edge*, **22**, 1038-1045.
- Vigrass, L.W., 1977, Trapping of oil at intra-Mannville (Lower Cretaceous) disconformity in Lloydminster area, Alberta and Saskatchewan: *American Association Petroleum Geologists Bulletin*, **61**, 1010-1028.